AIAA JOURNAL
Vol. 36, No. 6, June 1998

Shell Modeling of Fretting in Riveted Lap Joints

G. Harish* and T. N. Farris†
Purdue University, West Lafayette, Indiana 47907-1282

Fretting is a contact damage mechanism arising from microslip associated with small-scale oscillatory motion of nominally clamped structural members. Fretting has been observed near aircraft skin fastener holes. Shell finite elements are used to model the contact at a typical skin/rivet interface, with emphasis on fretting as a crack nucleation mechanism. Contact elements implementing the Coulomb friction law keep track of contact status between interacting surfaces. The model accounts for bending, contact between the skin panels, and rivet head clamping pressure. Elastic supports control the load transferred and simulate various rivet configurations. No interference is considered, leading to loss of contact between the skin and rivet on loading. The distinct stick-slip zones, combined with high tensile stresses at the edge of contact, are indicative of fretting, resulting in crack nucleation at the edge of contact. Away from the edge of contact, the tensile stress decays rapidly. The slip displacement has values typically associated with fretting fatigue. The interface between the two skin panels is also a region of fretting damage. Crack nucleation lives are predicted using a multiaxial fatigue theory. The top row of rivets has the smallest predicted life. For low remote stresses, increase in friction coefficient increases life, whereas for high remote stresses, life decreases with increase in coefficient of friction. Increasing rivet head clamping pressure increases the life. Plasticity blunts the effects of friction coefficient and clamping pressure. An approximate solution that does not require finite element analysis estimates the crack nucleation life for any rivet configuration quickly.

Introduction

FRETTING is a damage phenomenon occurring between contacting bodies nominally at rest but having oscillatory motion of small amplitude. Fretting is characterized by high contact stresses and microslip at the surface. Corrosion, wear, and fatigue all form part of the damage mechanism, which leads to acceleration of near-surface crack nucleation. Fretting has been well documented for flange joints, lap joints, dovetail notches in engine blades, roller bearings, and other locations exhibiting high contact stresses and small-scale oscillations.[1,2]

The fretting damage process can be divided into three stages.[3] In the first few cycles, the thin oxide layer resident on the material surface is removed through wear caused by the microslip. Then the material underneath the oxide layer forms microwelds through an adhesive process, accumulating wear debris between the contact surfaces.[4] Finally, the plastic deformation near the surface accumulates, and the wear process forms more oxide, which promotes the nucleation of microcracks. The coefficient of friction also increases during the first few hundred cycles and reaches a stable value.[5–7] Fretting fatigue results when one or more of these microcracks penetrate the bulk of the material. Fretting fatigue can reduce the crack nucleation life by an order of magnitude.

Because of various constraining factors, the U.S. Air Force is looking to extend the lives of some of its aging fleets of KC-135 and C-141. Also, some of the fleets are operating at loads higher than the design loads.[8] This has necessitated the periodic inspection of aircraft, both old and new. Particular emphasis is being laid on the effect of multiple site damage (MSD), which is characterized by a multitude of small cracks, which, although individually not catastrophic, can cause premature failure by their combined effects. Farris et al.[9] have discussed fretting as a mechanism for formation of MSD at fastener holes. The teardown inspections of KC-135, C-5A, and C-141 have revealed the existence of MSD cracks at fastener holes. This makes the understanding of various crack nucleation and propagation mechanisms very important. Figure 1 shows a typical lap joint and the local contact at a fastener location with the fretting locations highlighted. The nature of the contact between the skin and rivet, as well as between the two skin panels, is conducive to fretting damage, thus requiring a careful study of the parameters involved in fretting and the development of an appropriate theory applicable to actual structural members. In the recent past, various researchers have studied the fretting of lap joints in the laboratory.[10–12] Ghosh et al.[13] used an inverse method to study the load transfer from a smooth elastic pin onto an infinite sheet. Sundarraj et al.[14] used an axisymmetric model to study a double lap joint with no contact separation. Fung and Smart[15] analyzed a single-rivet lap joint. The current work investigates a typical lap splice with emphasis on fretting and an estimation of the effect of the fretting contact stresses on crack nucleation life.

Finite Element Model

Any theory must satisfy two criteria: It must agree with experimental results and must have a good physical basis. Although experiments simulating field behavior provide a framework for evaluating the theory, the physical basis involves the identification and proper modeling of the various parameters that govern the field phenomenon whose understanding is sought. The study of crack nucleation in lap joints is governed by the stress and strain state in the joint as well as the material properties of the components. The present work concentrates on the estimation of the stresses and strains and their effect on the crack nucleation behavior for a joint made of 2024-T351 aluminum with a Young's modulus of 73 GPa and a Poisson's ratio of 0.33. A bilinear kinematic hardening model is used to model plasticity, with an initial yield stress of 330 MPa and a hardening modulus E_t of 1.55 GPa. Because the state of stress is influenced by the complex phenomena of contact and plasticity (and their interactions with each other), closed-form solutions are not available. The finite element method (FEM) is a numerical approach to such problems.

The finite element approach involves the following steps: identification of the skin/rivet configurations to be studied, reduction to a discrete model with necessary assumptions, solution of the discrete model for various loading patterns, and interpretation of the results within the framework of assumptions.

The model consists of one-half rivet and the skin around it. A finite number of rivet rows, with a large number of rivets in each row, is assumed. The section of the plate near the lap joint may be considered equivalent to a collection of unit structures, each of which is similar to the model, comprising half a rivet and the adjacent skin around it.

Presented as Paper 97-1340 at the AIAA/ASME/ASCE/AHS/ASC 38th Structures, Structural Dynamics, and Materials Conference, Kissimmee, FL, April 7–10, 1997; received June 19, 1997; revision received Jan. 30, 1998; accepted for publication Feb. 9, 1998.

*Research Assistant, School of Aeronautics and Astronautics, 1282 Grissom Hall #350.

†Professor, School of Aeronautics and Astronautics, 1282 Grissom Hall #350. Senior Member AIAA.

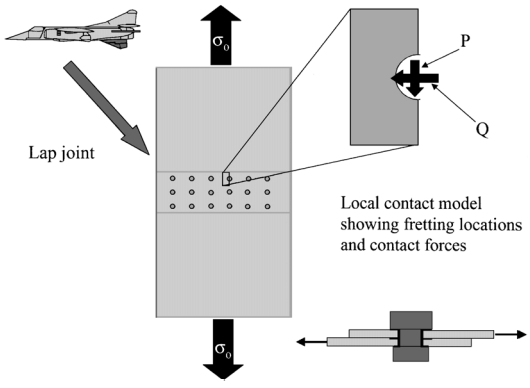

Fig. 1 Fretting and aircraft.

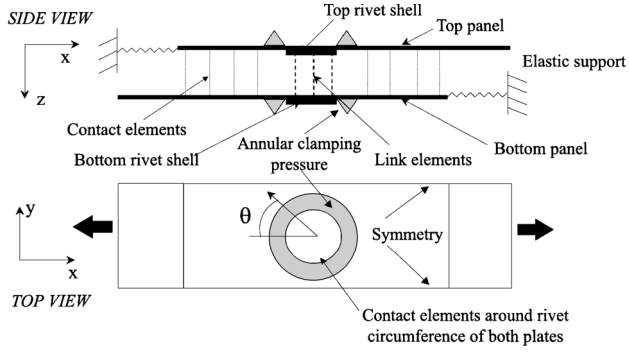

Fig. 2 Schematic of shell model.

The remote load seen by each rivet is uniformly distributed on the model boundaries. Appropriate boundary conditions and spring elements allow for the modeling of any particular rivet with arbitrary load transfer. The results in this work refer to a three-row lap joint containing rivets of diameter 0.51 cm with a spacing of 2.54 cm. The effect of rivet head clamping is accounted for by applying an annular pressure on the skin around the rivet. The contact regions comprise the skin/rivet interface and the skin/skin interface.

The dimensions of aircraft skin panels are characteristic of the realm of validity of shell theory. The two skin panels are modeled as shells. To ensure consistency of the model, the rivet too is modeled as two shells initially aligned with the skin shells. These two shells are subjected to constraint conditions to link them together. Each skin panel is 7.62 cm in length and 1.27 cm in width. The thickness of each panel is 1.78 mm. Figure 2 shows a schematic of the model. Considering the effect of local contact stresses to be negligible at a distance of five radii (of the rivet) from the contact, the remote load is distributed uniformly along the edges of the two panels. Both of the panels have symmetry conditions along the edges parallel to the applied remote loading, which follows from the assumption of an infinite number of rivets in each row. Consequently, a nonuniform traction, orthogonal to the applied remote load, results on the application of the remote traction. There are elastic supports on one side of either panel. By varying the stiffness of the support, the amount of load being transferred by the rivet assembly can be controlled. This, coupled with the magnitude of the applied remote traction, enables the simulation of any configuration having an arbitrary number of rows of rivets. The elastic supports model the effect of the subsequent rows of rivets, whereas the magnitude of the applied traction takes into account the load transferred in the rows ahead of the rivet being analyzed.

The sum of the applied traction and the support reaction must be the same for both of the shells. Hence, the support stiffnesses are not arbitrary but must be found iteratively. The clamping pressure due to the rivet head on the skin panels is modeled by applying pressure on an annular region bounded by the rivet hole and an outer circle with radius 1.3 times the radius of the rivet.[16] The pressure goes to zero on either end to ensure a smooth profile. The total force acting on the top and bottom shell is equal. Note that this is the clamping pressure that remains after the removal of the forces applied during the installation of the rivet.

To enable the two distinct shells composing the rivet to behave as a single body, link elements and constraint equations are used. The link elements link the corresponding nodes of the top and bottom shells. The nodes are located in the midplane of the shells. Both of the shells have identical meshes for this purpose. The two nodes on either shell are connected by a rod element that has a stiffness determined by the stiffnesses of each of the elements that contain the two nodes that form the rod element. Each shell element would contribute a stiffness, the value of which depends on the element volume and the number of nodes in the element, to each of the nodes that compose it. The stiffnesses are summed at each node, and the stiffness of the rod element is then determined. For identical meshes of the two shells with the same thickness, the equation for the stiffness can be expressed as

$$K = \frac{1}{t}\sum \frac{A_i E_i}{n_i} \qquad .1/$$

where K is the stiffness, t is the thickness, A_i and E_i are, respectively, the area and the Young's modulus of the elements that are connected to the node, and n_i is the number of nodes in the element. Note that only one of the link element nodes needs to be considered for the preceding equation, and the summation is over all of the elements containing the node.

The bottom of the top rivet shell and the top of the bottom rivet shell correspond to the same point in physical space. Hence, constraint equations are imposed to ensure continuity at this plane, the center plane of the rivet itself. The constraint equations account for translation and bending of the shell as well as any shear deformation. The two equations at each node pair corresponding to the two in-plane directions can be expressed as

$$.u_i + 0{:}5\mu_i t/_{\text{bottom}} = .u_i - 0{:}5\mu_i t/_{\text{top}} \qquad .2/$$

where t is the thickness of each of the shells forming the rivet, u_i is the translational displacement in the i direction, and μ_i is the angular displacement (in the i direction) of the normal section to the midplane of the shell.

Contact Modeling

Contact elements are used to keep track of the contact between the various surfaces. Contact elements exhibit a nonlinear relationship between force and displacement. They have zero stiffness in tension and a high stiffness in compression. In the present model, contact elements are used to keep track of the contact between the skin and rivet as well as between the two skin panels themselves. Point-to-point contact elements are used for both contacts. Even though the problem is three dimensional, the nature of contact is roughly the same over the entire loading spectrum. Also, the sliding is expected to be small. Hence, because the contact area can be estimated a priori, the point-to-point contact elements are the most appropriate.

The contact elements between the two shells have a soft contact stiffness. This allows the two nodes composing the contact element to move toward each other in compression, simulating the compression of the two skin panels in the transverse direction. The contact stiffness is calculated using the method used to calculate the stiffness for the link elements connecting the rivet shells. The contact stiffness for the contact elements between the plate and rivet is kept high in comparison to the stiffness of the adjacent shell elements.

The shell element has only one node through the thickness. Hence, contact can be resolved only at the midplane of the shell. Partial contact through the thickness cannot be resolved. Bending effects are not considered as part of the contact forces. Figure 3 shows an example of a possible contact state and the finite element implementation of the same.

Finite Element Mesh

The commercial finite element package, ANSYS version 5.3, provided to Purdue University on an academic license, is used for the solution of the problem. The skin panels and the rivet shells are modeled by four-noded Mindlin shell elements (SHELL43). The contact

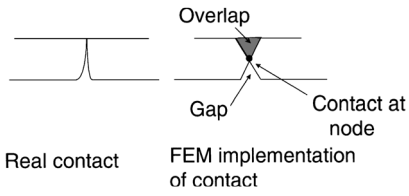

Fig. 3 Implementation of contact in FEM.

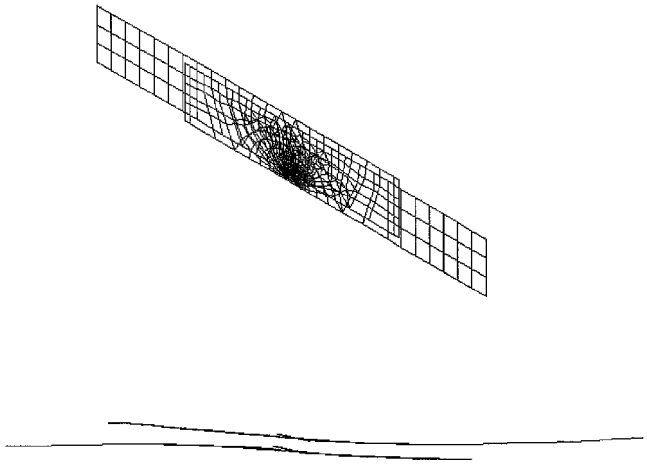

Fig. 4 Finite element mesh (on top) with side view of deformed mesh: σ_o = 96.5 MPa, μ = 0.65, maximum clamping pressure = 83 MPa, and LTR = 0.38.

elements are three-dimensional, point-to-point elements (CONTAC52). The two rivet shells are linked by rod elements (LINK4). The finite element mesh is shown in Fig. 4. There are 852 nodes composing 768 shell elements. There are 24 elements around the circumference of the rivet. The contact is tracked through 267 contact elements. There are 50 contact elements between the panel and rivet shells and 217 contact elements between the two panels. There is a row of elements on each panel shell that acts as the elastic support modeling the effects of the subsequent rows of rivets. These provide both axial and bending stiffness. There are symmetry conditions on the boundaries parallel to the x axis. Tractions are applied along one edge of each of the two panels parallel to the y axis. Displacement compatibility is imposed on the rivet shells using Eq. (2).

Five remote stresses from 55 to 110 MPa, three coefficients of friction (0.2, 0.4, and 0.65), and two values of maximum clamping pressures (55 and 83 MPa) were investigated. These analyzes were performed assuming the joint of interest to be the first row of a three-lap joint with 38% of applied remote load transferred through the rivet. Also, the corresponding configuration of the second row with 24% load transfer was studied.

Verification of Mesh Adequacy

The first step in the analysis is to verify that the mesh is able to resolve the contact and other issues accurately. The problem was solved with zero load transfer and no friction. The symmetry condition modeling the infinite number of rivets is replaced by an applied traction. Because the boundaries are far away from the rivet, their effect is small. The results were compared with the solution for a frictionless inclusion in an infinite matrix. Note that this is a receding contact problem. The analytical solution is due to Keer et al.[17] The results are shown in Fig. 5 for two ratios of the tractions along the two directions. The finite element results agree well with the analytical solution, demonstrating the adequacy of the mesh.

Results

The displacement profile is shown in Fig. 6, and a side view of a typical displacement profile is shown at the bottom of Fig. 4. The contact is centered around $\mu = 0$ deg with the half-contact angle calculated to be approximately 90 deg. The dominant contact mechanism is seen to be the global motion of the skin into the rivet. Another mechanism is the tendency of the skin panel hole to

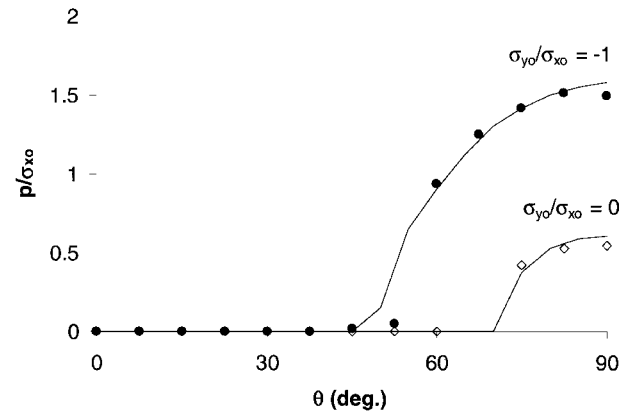

Fig. 5 Comparison of results for 0 LTR case with analytical solution.

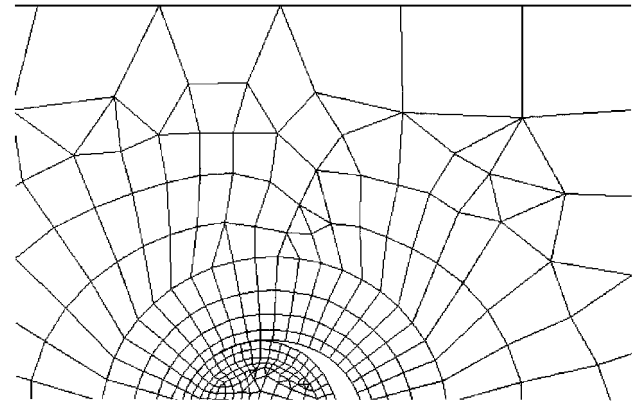

Fig. 6 Top view of deformed mesh (only a portion of the mesh is shown for clarity): σ_o = 96.5 MPa, μ = 0.65, maximum clamping pressure = 83 MPa, and LTR = 0.38.

deform into a elliptical shape under loading, which contributes to the contact around $\mu = 90$ deg. The observed contact area is in agreement with the results of Narayana and Dayananda.[18] The contact area is observed to be nearly constant for all values of the applied load, especially with little or no plasticity. This surprising result can be explained by considering the nature of the skin/rivet contact. Because the final contact area is less than the initial contact area (with no load), this problem is a receding contact problem. It can be shown that, for such problems, the contact area is independent of the actual magnitudes of the applied loads.[19] Whereas the preceding result assumes elastic behavior, the present problem has little plasticity, and hence the contact area remains constant.

The load transferred through the rivet assembly is transferred through the skin/skin interface and between the skin/plate interface. The partition of load between the rivet and skin/skin interface is shown schematically in Fig. 7. When the loading is applied for the first time, initially nearly all of the load is taken up by the interfacial friction as the panels have to overcome this interfacial friction to move into the rivet and initiate contact at the rivet/skin interface. Thus, the rivet begins to take up load only after the two panels slip with respect to each other. The rivet absorbs the subsequent loading. When unloading begins, once again the panels need to slip in the opposite direction to relieve the load on the rivet. This necessitates the reversal of the interfacial frictional load. During this phase of unloading, the rivet itself does not experience significant change in load. When the unloading is complete, there is a frictional load between the two panels and a balancing load on the rivet. When reloading begins, once again the interfacial friction accounts for the initial part and the rivet absorbs the subsequent loading. This mechanism now continues in a cyclic fashion. The amount of interfacial friction depends on the clamping pressure on the rivet. Also, the presence of high slip amplitudes in conjunction with any high stresses can cause extensive damage to the faying surfaces and nucleate cracks.

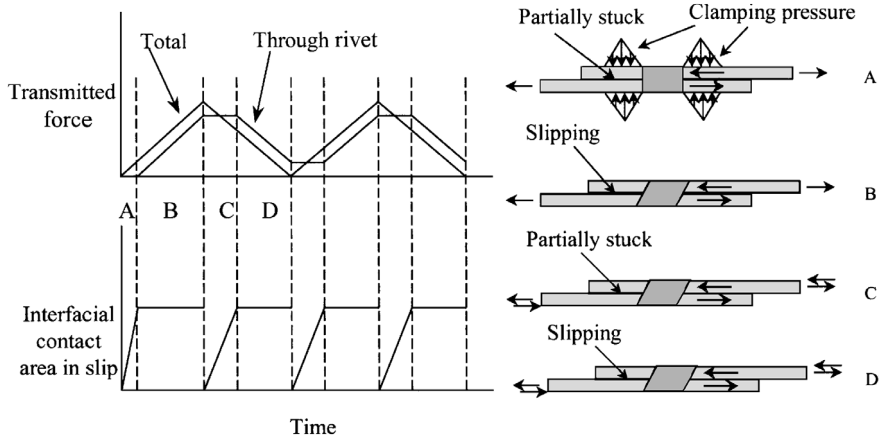

Fig. 7 Partition of load between rivet and interfacial friction between panels.

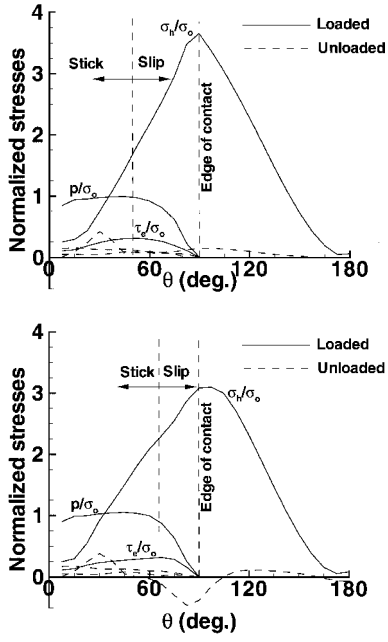

Fig. 8 Contact stresses, elastic regime: σ_o = 83 MPa, μ = 0.4, maximum clamping pressure = 83 MPa, and LTR = 0.38.

Fig. 9 Contact stresses, plastic regime: σ_o = 110 MPa, μ = 0.4, maximum clamping pressure = 83 MPa, and LTR = 0.38.

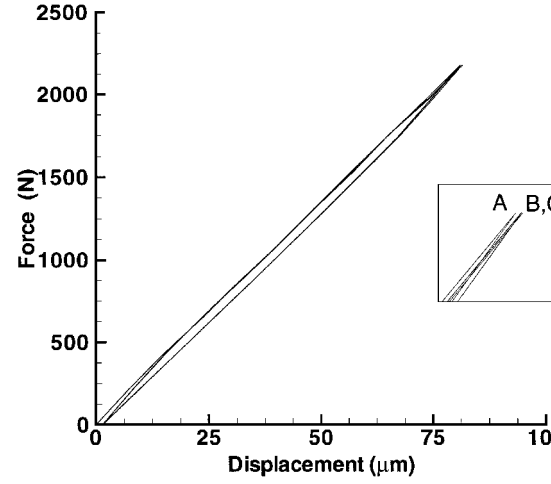

Fig. 10 Hysteresis diagram over two and a half cycles; A, B, and C are consecutive peak loadings: σ_o = 96.5 MPa, μ = 0.65, and maximum clamping pressure = 83 MPa. Data are plotted for top panel, first row.

Evidence of Fretting

The most severe stress conditions occur at the skin/rivet interface for the parameters considered in the present study. Figure 8 shows the results, expressed in the form of stress distribution around the rivet hole, for a typical configuration. Figure 9 shows similar results for a loading configuration that produces plastic deformation. The normal pressure p, the equivalent shear stress ¿eq at the interface, and the hoop stress on the panel surface are plotted as functions of the angular coordinate μ, which is defined in Fig. 2. The stresses, plotted at the midplane of the shell (without bending effects), are made nondimensional by dividing by the remote tensile load ¾o. The loaded and unloaded configurations are plotted. The stick/slip nature of the contact is observed, where slip is characterized by the frictional contact force being equal to the coefficient of friction times the normal contact force. Note that, because the contact algorithm uses only forces, the effective coefficient of friction when comparing shear and normal stresses in the slip zone might be different. This effective coefficient of friction is referred to as ¹eff. The stick/slip nature is also verified by checking the nature of the contact elements. Wherever the contact elements report no contact, the pressure and shear traction are assumed to be zero.

The pressure distribution is nearly semielliptic in nature and resembles the Hertzian pressure distribution. However, at higher load transfer ratios (LTR; the ratio of transferred load to applied remote load), the pressure reaches a maximum at a value of μ other than zero, an effect of the aforementioned effect of the local tendency of the panel hole to deform into an ellipse. This causes the region around μ = 0 deg to move away from the rivet, with a resulting drop in the contact pressure. The effective shear stress, which is the vector sum of the two interfacial shear stresses ¿rμ, and ¿rz, follows the pressure distribution in the slip region, where ¿eq equals ¹eff p. In the stick region, the effective shear stress decreases as μ goes to zero. The region of slip varies from 60 to 15 deg of arc as the coefficient of friction varies from 0.2 to 0.65. Experiments indicate that for 2024-T351 aluminum the coefficient of friction is about 0.2 initially and under fretting conditions increases to a stable value of about 0.65 after a few hundred cycles.

The hoop stress ¾h has a peak at the edge of contact, i.e., μ = 0 deg, and decays rapidly away from the edge of contact. However, it seems to stabilize in the stick region. The hoop stress is derived from three sources: the stress concentration due to the panel hole, the normal pressure, and the shear traction. The latter two result from contact.

In Fig. 9 the same features mentioned earlier are observed, except that plasticity causes the hoop stress distribution around the edge of contact to be flatter as the load gets redistributed. The pressure distribution is also flatter and no longer resembles the Hertzian distribution. The plasticity is very localized and is observed only in the first cycle. Owing to the small strain hardening, the peak value of stress remains close to the nominal yield stress. Additionally, the adjacent elastic material constrains the plastic deformation. Subsequent loading cycles are elastic, cycling between the two states shown in Fig. 9. Figure 10 shows a hysteresis plot of the applied remote load against the displacement in the direction of the load at the loading edge of the top panel. The first cycle includes plastic energy dissipation in addition to the frictional energy dissipation. The subsequent cycles marked B and C are identical, indicating that there is no further plastic energy dissipation. The area enclosed by the hysteresis curve over one cycle gives the energy dissipation for that cycle.

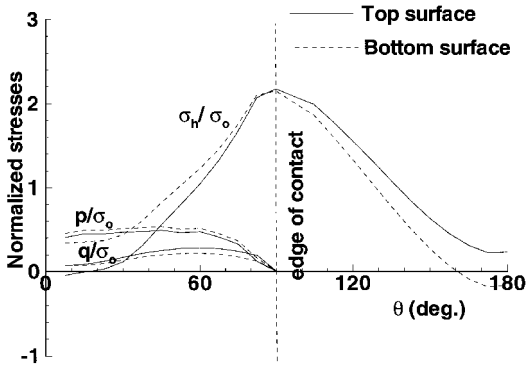

Fig. 11 Contact stresses, bending effects: σ_o = 96.5 MPa, μ = 0.65, maximum clamping pressure = 83 MPa, and LTR = 0.24 (middle row).

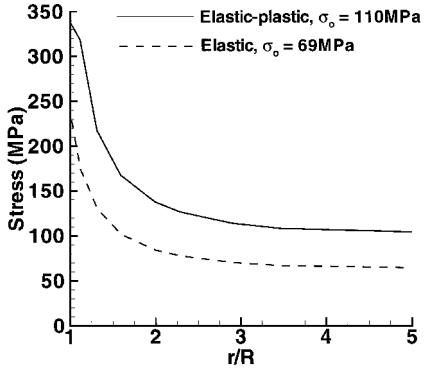

Fig. 12 Decay of σ_h in radial direction; R is the radius of the rivet: μ = 0.2 and LTR = 0.38.

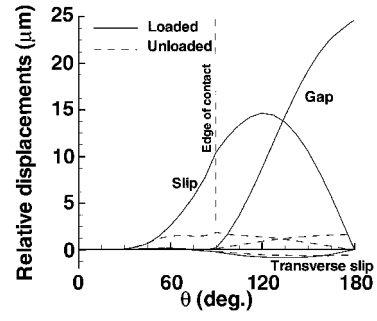

Fig. 13 Relative displacements between skin and rivet: σ_o = 96.5 MPa, μ = 0.65, maximum clamping pressure = 83 MPa, and LTR = 0.38 Data are plotted for top panel, first row.

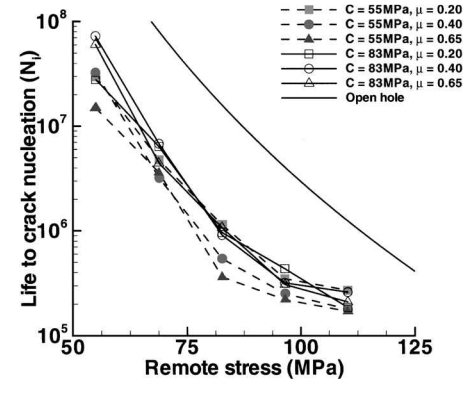

Fig. 14 Crack nucleation lives at various remote stresses and clamping pressures.

As mentioned earlier, on unloading, the pressure and other stresses do not go to zero. In the presence of plasticity, the hoop stress at the edge of contact is compressive on unloading. The cyclic stress in the rivet is the difference between the stable loaded and unloaded configurations. The presence of distinct stick-slip zones in the contact area, coupled with the high tensile hoop stress at the edge of contact, is indicative of fretting behavior.

Figure 11 shows the effect of local bending on the contact stresses between the rivet and skin. Although bending affects all three contact stresses, the effect on the hoop stress is minimal at the edge of contact, which is the critical location. Hence, stress severity at the critical location is unaffected by local bending. In the slip region, ¿eq is not equal to $^{1}{}_{\text{eff}}p$, as the contact algorithm uses the contact force at discrete nodes and does not account for the bending forces, in contrast to the stress-based approach more suitable for continuum bodies.

The rapid decay of the hoop stress away from the contact interface is shown in Fig. 12 . Both the contact stresses and the stress concentration decay rapidly away from the hole. The gradient is quite steep even when plasticity sets in. Thus, this problem involves high stress gradients in addition to contact, frictional dissipation, and plasticity. The decay of the stresses along the 0-deg direction is steep as well, resulting in a nearly uniform state of stress at the elastic supports. This indicates that rivet interaction is primarily through stress shielding, which is simulated through the use of appropriate boundary conditions.

Fretting fatigue occurs when slip displacements between the panels and the rivet are small. Figure 13 shows the relative displacements between the top panel and the corresponding rivet shell. The gap displacement refers to the relative normal displacements between the plate and rivet. This is zero in the contact region. The gap is positive elsewhere, indicating loss of contact. The slip displacement refers to the relative motion between the plate and rivet in the hoop direction. The slip in the transverse direction is also brought out in the model. The transverse slip is small in the presence of clamping pressure on the rivet head, in part due to the consequent restriction on the motion of the plate in the thickness direction. The slip displacements are zero in the stick region and indicate the amount of slip in the slip region. Once again the stable value of the slip is nonzero in the unloaded state. The slip displacement plot has no particular significance beyond the contact area. The maximum slip displacement occurs at the edge and typically is nearly 14 ^{1}m. This is consistent with the values reported for a lap joint.[20] This small slip causes wear that nucleates a crack at the edge of contact, which is then driven by the tensile hoop stress. Thus, this is the critical location for a crack to nucleate. The slip between the two panels reaches a maximum of 1:5 ^{1}m at $\mu = 135$ deg and a radial distance of 1.6 from the center of the hole, where R is the hole radius. This slip may be related to the formation of cracks at the skin/skin interface away from the skin/rivet contact.

Application to Fretting Crack Nucleation

The multiaxial theory proposed by Socie[21] has been used by Szolwinski and Farris[22] to predict fretting crack nucleation in a controlled fretting test. Their predictions are in good agreement with the experiments of Nowell and Hills[23] and data collected at Purdue University.[24] The number of cycles N_i to nucleate a crack of length 1 mm is given by

$$0 = ¾_{\max}.1^{2}=2/ = \left(¾_f'^{2}/E\right).2N_i l^{2b} + ¾_f'^{2}{}_f.2N_i l^{b+c} \qquad .3/$$

where the fatigue constants $¾_f'$; $^{2}{}_f$; b, and c are 1013.5 MPa, 0.22, −0:12, and −0:52. The critical parameter is identified as 0, the maximum value of the product of the maximum stress and the normal strain amplitude. This always occurs near the edge of contact for lap joints without interference. Note that, for uniaxial loading, Eq. (3) becomes the Smith–Watson–Topper equation.[25] The predicted lives to crack nucleation are shown in Fig. 14. Any other life prediction theory would give similar qualitative results with possible scale changes. For the middle row of rivets, the stress level is much lower than that for the first row of rivets. Only the first row results are plotted, as the middle row data fall above the open hole data. The load transfer ratio is kept at 0.38. The open hole data are for a plate with no hole subjected to the same remote loading. The effects of friction, clamping pressure, and plasticity are discussed next.

Effects of Coefficient of Friction

As the coefficient of friction increases, the region of stick becomes larger and results in more shear traction, which increases the hoop stress at the edge of contact. For a given load transfer ratio of the rivet assembly, as the coefficient of friction increases, there is more load taken up by the interfacial friction between the two skin panels, resulting in less load being transferred through the rivet itself. The tradeoff is that the higher coefficient of friction increases the severity of the local stresses at the skin/rivet contact for a given load. For small remote loads, the load reduction is more than that required to compensate for the increased stress severity, resulting in lower stress values overall. As the remote load increases, the load relief provided by the increased interfacial friction is insufficient to offset the high stress severity. Also, as the coefficient of friction increases for a given remote stress, the interfacial frictional load once again cannot compensate for increased stress severity. There is an optimum coefficient of friction for a given configuration. In a lap joint, the coefficient of friction is expected to stabilize after a few cycles, and hence the application of the preceding phenomenon lies in using coatings to reduce friction. It might be more beneficial to reduce friction at the skin/rivet interface but let the friction develop between the two panels.

At low remote loads, an increased coefficient of friction is beneficial in increasing the crack nucleation life. This beneficial effect becomes less pronounced either as the remote stress increases or as the coefficient of friction becomes very high. At high remote loads, plasticity sets in and constrains the value of peak stress, causing any effects of friction to be blunted.

Effects of Clamping Force

As seen from Fig. 7, the clamping pressure determines the load taken up by interfacial friction between the panels, which reduces the load taken up by the rivet and hence the stress severity at the skin/rivet interface. The two clamping conditions considered correspond to a clamping force of 930 and 1400 N. The clamping pressure diffuses through the thickness and encompasses a larger area at the interface of the two panels. The interfacial friction needs to be overcome before any change in the load transferred through the rivet takes place. The higher the clamping pressure, the greater the interfacial frictional load, and, hence, the less the load on the rivet. This results in lower peak stress values leading to higher nucleation lives as shown in Fig. 14. Again, this effect is less significant in the presence of plasticity.

Effects of Plasticity

The observed plasticity is restricted to a small zone near the edge of contact. The sharp peak in the hoop stress initiates plastic deformation in the first loading cycle. The constraining effect of the surrounding elastic material coupled with the small strain hardening of aluminum causes the plastic deformation to remain small with any additional load being redistributed. The peak stress values remain close to the nominal yield stress. There is no change in the contact area. On unloading, the hoop stress becomes negative close to the edge of contact, and subsequent cycles oscillate between this state and the stress state on reloading. This is demonstrated by the hysteresis plot (Fig. 10). However, the strain amplitude is still comparable to the values obtained in a purely elastic analysis. Hence, as Eq. (3) uses the maximum stress as a parameter, plasticity reduces the value of 0 and hence the crack nucleation life curve flattens out at high remote stresses. In addition, plasticity blunts the effects of increased coefficient of friction and clamping force. However, if a pure-strain-amplitude-based theory is used, plasticity will not have such a significant effect.

Approximate Model

The origin of the stress concentration at the skin/rivet contact can be identified as the combination of the stress concentration due to the rivet hole and the contact stresses. For the purpose of an approximate solution, it may be assumed that the two contributions can be superposed. Whereas the stress concentration can be approximated as a plate with a hole under tension with symmetry boundary conditions along the edges parallel to the tensile traction, the contact problem is symmetric about $\mu = 0$ deg and does not have a closed-form solution. However, the corresponding antisymmetric problem (Mindlin problem) has a closed-form solution.[26] The presence of an antisymmetric boundary condition as opposed to a symmetric boundary condition has a small effect at the edge of contact. McVeigh and Farris[27] have shown that the Mindlin solution can be used to approximate more complicated situations involving stress due to other sources in addition to contact stresses. Hence, the preceding approach is appropriate to estimate the stress (and strain) at the edge of contact. Figure 15 shows the schematic decomposition of the problem into a stress concentration and Mindlin problem with the same contact area, normal force, and slip zone. Bending is neglected as it has little effect at the edge of contact. The interfacial friction is assumed to take up a load of $^{1}{}_{\text{eff}}F$, where F is the clamping force.

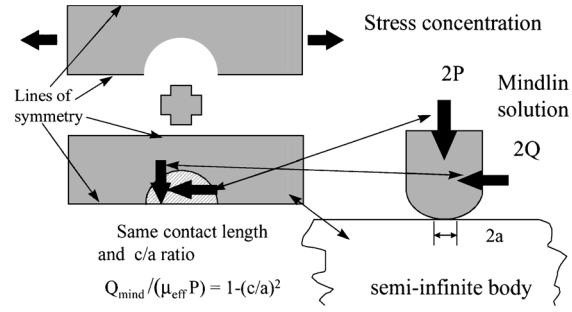

Fig. 15 Analytical equivalent of skin/rivet contact.

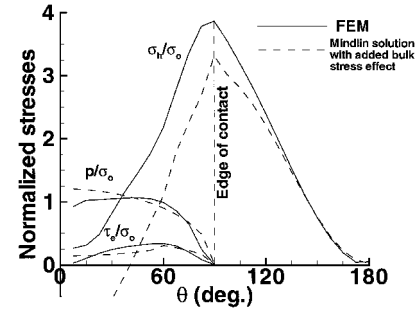

Fig. 16 Comparison of FEM and analytical contact stresses: σ_o = 83 MPa, $\mu = 0.4$, maximum clamping pressure = 55 MPa, and LTR = 0.38 (top panel, first row).

Figure 16 shows the comparison of the finite element solution and the analytical approximation for a particular loading case. The agreement is best near the edge of contact, and the analytical solution degrades as we move away. Whereas the Mindlin solution assumes a Hertzian pressure distribution, the tendency of the hole to deform into an ellipse forces the actual pressure distribution to look different. Also, for the Mindlin problem, the shear stress does not go to zero at $\mu = 0$ deg.

Because a finite element analysis cannot be done for every possible configuration, the parameter governing crack nucleation 0 is quickly estimated as follows. The load transfer ratio, remote stress, clamping pressure, and coefficient of friction are assumed to be known. The interfacial frictional force is calculated, and the load taken up by the rivet is obtained. The ratio of stick zone length to total contact length is assumed to be equal to the coefficient of friction itself. The normal force and the frictional force can be calculated from the remote stress, the load transfer ratio, and the rivet dimensions. The stress concentration (including the symmetry tractions) and the contact stress can now be estimated. A perfectly plastic material is assumed, and the strain amplitude is calculated as if the material were elastic. The details of this implementation can be found in Ref. 28. Figure 17 shows the comparison of the finite element and analytical values of 0 for all of the cases studied. The correlation is good considering the approximations made in the theoretical model. This approximation may be used with Eq. (3) to predict crack nucleation quickly.

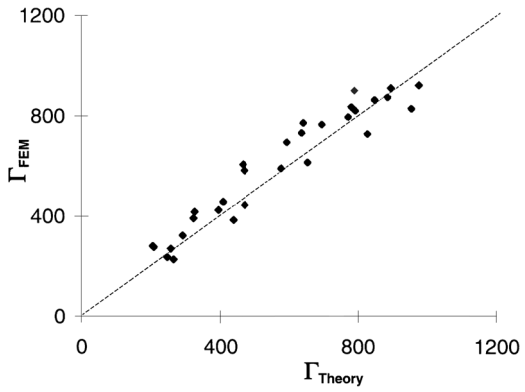

Fig. 17 Comparison of Γ: FEM and theory.

Conclusions

Fretting is one of the causes of crack nucleation in riveted lap joints. For riveted lap joints with no interference, fretting damage can occur at the skin/rivet interface as well as at the interface between the two skin panels. The finite element method has been used to demonstrate the prevalence of conditions conducive to fretting damage. The effects of friction, rivet head clamping pressure, and plasticity are accounted for in a shell model. Higher clamping force causes more load to be taken up at the skin/skin interface, thereby reducing the load on the rivet itself. This also causes the rivet to have some residual load on unloading. A higher coefficient of friction causes more severe contact stresses at the skin/rivet interface but also increases the frictional load-bearing capacity of the skin/skin interface, causing some relief in the load seen by the rivet. There is an optimum coefficient of friction at which the stress severity for a given configuration is minimum. Plasticity constrains the peak value of the stresses at the edge of contact, which is the primary location for the cracks nucleated by the relative slip between the skin and rivet and propagated by the high stresses at the edge of contact. A multiaxial fatigue model based on the Smith–Watson–Topper equation is used to predict the number of cycles to nucleate a fretting crack at the edge of contact. The first row of rivets in a multirow lap joint are the most susceptible to fretting crack nucleation as they transfer more load and are subject to higher stress concentration. A simple model is used to quickly estimate the crack nucleation life for an arbitrary lap joint.

Acknowledgment

This research is sponsored by the U.S. Air Force Office of Scientific Research through Contract F49620-93-1-0377.

References

[1]Kalb, B. J., "Friction Stresses Between Blade and Disk Dovetail Possible Cause of Numerous Dovetail Problems," *Proceedings of the 1991 USAF Structural Integrity Program Conference*, Wright Lab., Wright–Patterson AFB, OH, 1991, pp. 585–601.

[2]Waterhouse, R. B., "Fretting Fatigue in Aqueous Electrolytes," *Fretting Fatigue*, Applied Science, London, 1981, pp. 159–176.

[3]Hurricks, P. L., "Mechanism of Fretting," *Wear*, Vol. 15, 1970, pp. 389–409.

[4]Waterhouse, R. B., and Taylor, D. E., "The Initiation of Fatigue Cracks in a 0.7% Carbon Steel by Fretting," *Wear*, Vol. 17, 1971, pp. 139–147.

[5]Hills, D. A., Nowell, D., and O'Connor, J. J., "On the Mechanics of Fretting Fatigue," *Wear*, Vol. 125, 1988, pp. 129–146.

[6]Nishioka, K., and Hirakawa, K., "Fundamental Investigations of Fretting Fatigue, Part 2," *Bulletin of the Japan Society of Mechanical Engineers*, Vol. 12, No. 50, 1969, pp. 180–187.

[7]Endo, K., and Goto, H., "Initiation and Propagation of Fretting Fatigue Cracks," *Wear*, Vol. 38, 1976, pp. 311–324.

[8]Lincoln, J., "USAF Aging Aircraft Program," *Aerospace Engineering*, Vol. 34, No. 10, 1994, pp. 11–13.

[9]Farris, T. N., Grandt, A. F., Harish, G., and Wang, H. L., "Analysis of Widespread Fatigue Damage in Structural Joints," *41st International SAMPE Symposium and Exhibition*, Society for the Advancement of Material and Process Engineering, Covina, CA, 1996, pp. 65–79.

[10]Iyer, K., Hahn, G. T., Bastias, P. C., and Rubin, C. A., "Analysis of Fretting Conditions in Pinned Connections," *Wear*, Vol. 181, 1995, pp. 524–530.

[11]Petiot, C., Vincent, L., Dang Van, K., Maouche, N., Foulquier, J., and Journet, B., "An Analysis of Fretting–Fatigue Failure Combined with Numerical Calculations to Predict Crack Nucleation," *Wear*, Vol. 181, 1995, pp. 101–111.

[12]Müller, R. P. G., "An Experimental and Analytical Investigation on the Fatigue Behavior of Fuselage Riveted Lap Joints," Ph.D. Thesis, Dept. of Aerospace Engineering, Delft Univ. of Technology, Delft, The Netherlands, 1995.

[13]Ghosh, S. P., Dattaguru, B., and Rao, A. K., "Load Transfer from a Smooth Elastic Pin to a Large Sheet," *AIAA Journal*, Vol. 19, No. 5, 1981, pp. 619–625.

[14]Sundarraj, N., Dattaguru, B., and Ramamurthy, T. S., "Analysis of a Double Shear Lap Joint with Interference Fit Pin," *Computers and Structures*, Vol. 55, No. 2, 1995, pp. 357–363.

[15]Fung, C. P., and Smart, J., "An Experimental and Numerical Analysis of Riveted Single Lap Joints," *Proceedings of the Institution of Mechanical Engineers, Journal of Aerospace Engineering*, Vol. 208, 1994, pp. 79–90.

[16]Reithmaier, L. (ed), *Standard Aircraft Handbook*, 4th ed., Tab Books, Blue Ridge Summit, PA, 1986, Chap. 1.

[17]Keer, L. M., Dundurs, J., and Kiattikomol, K., "Separation of a Smooth Circular Inclusion," *International Journal of Engineering Science*, Vol. 11, No. 11, 1973, pp. 1221–1233.

[18]Narayana, K. B., Dayananda, T. S., Dattaguru, B., Ramamurthy, T. S., and Vijayakumar, K., "Cracks Emanating from Pin-Loaded Lugs," *Engineering Fracture Mechanics*, Vol. 47, No. 1, 1994, pp. 29–38.

[19]Dundurs, J., "Properties of Elastic Bodies in Contact," *Proceedings of the Symposium of the International Union of Theoretical and Applied Mechanics*, edited by A. D. de Pater and J. J. Kalker, Delft Univ. Press, Delft, The Netherlands, 1974, pp. 54–66.

[20]Harris, W. J., *Metallic Fatigue*, Pergamon, New York, 1961, pp. 166–204.

[21]Socie, D., "Critical Plane Approaches for Multiaxial Fatigue Damage Assessment," *Advances in Multiaxial Fatigue*, ASTM STP 1191, American Society for Testing and Materials, Philadelphia, PA, 1993, pp. 7–36.

[22]Szolwinski, M. P., and Farris, T. N., "Mechanics of Fretting Fatigue Crack Nucleation," *Wear*, Vol. 198, 1996, pp. 93–107.

[23]Nowell, D., and Hills, D. A., "Crack Initiation Criteria in Fretting Fatigue," *Wear*, Vol. 136, 1990, pp. 329–343.

[24]Szolwinski, M. P., Harish, G., McVeigh, P. A., and Farris, T. N., "The Role of Fretting Crack Nucleation in the Onset of Widespread Fatigue Damage: Analysis and Experiments," *Proceedings of the FAA–NASA Symposium on the Continued Airworthiness of Aircraft Structures* (Atlanta, GA), Office of Aviation Research, Washington, DC, 1996, pp. 585–596.

[25]Smith, K. N., Watson, P., and Topper, T. H., "A Stress–Strain Function for the Fatigue of Metals," *Journal of Materials*, Vol. 5, No. 4, 1970, pp. 767–778.

[26]Mindlin, R. D., and Deresiewicz, H., "Elastic Spheres in Contact Under Oblique Forces," *Journal of Applied Mechanics*, Vol. 75, Sept. 1953, pp. 327–344.

[27]McVeigh, P. A., and Farris, T. N., "Finite Element Analysis of Fretting Stresses," *Journal of Tribology*, Vol. 119, 1997, pp. 797–801.

[28]Harish, G., and Farris, T. N., "Modeling of Skin/Rivet Contact: Application to Fretting Fatigue," *A Collection of Technical Papers, AIAA/ASME/ASCE 38th Structures, Structural Dynamics, and Materials Conference*, Vol. 4, AIAA, Reston, VA, 1997, pp. 2761–2771.

R. K. Kapania
Associate Editor